PCCP

PAPER

Check for updates

The 2D or 3D morphology of sub-nanometer Cu$_5$ and Cu$_8$ clusters changes the mechanism of CO oxidation†

Estefanía Fernández, [ID] Mercedes Boronat [ID] * and Avelino Corma [ID]

The mechanism of the CO oxidation reaction catalysed by planar Cu$_5$, three dimensional (3D) Cu$_5$, and 3D Cu$_8$ clusters is theoretically investigated at the B3PW91/Def2TZVP level. All three clusters are able to catalyse the reaction with similar activation energies for the rate determining step, about 16–18 kcal mol^{-1}, but with remarkable differences in the reaction mechanism depending on cluster morphology. Thus, for 3D Cu$_5$ and Cu$_8$ clusters, O$_2$ dissociation is the first step of the mechanism, followed by two consecutive CO + O reaction steps, the second one being rate determining. In contrast, on planar Cu$_5$ the reaction starts with the formation of an OOCO intermediate in what constitutes the rate determining step. The O–O bond is broken in a second step, releasing the first CO$_2$ and leaving one bi-coordinately adsorbed O atom which reacts with CO following an Eley–Rideal mechanism with a low activation energy, in contrast to the higher barriers obtained for this step on 3D clusters.

Introduction

Sub-nanometre metal clusters composed by just a few atoms have emerged in the last few years as a specific type of nanomaterials with unexpected and finely tunable properties. Their molecule-like electronic structure composed by localized orbitals with discrete energy levels provides them with unforeseen catalytic properties, with many applications being already described for atomically precise Au, Ag, Pd or Pt clusters.[1–18] Nowadays, there is increasing interest on the catalytic behaviour of cheaper and abundant non-noble metals, like for instance Cu, and on the possibility of controlling their reactivity and stability using accurate synthesis procedures leading to a specific atomicity.

Due to their ability to activate and dissociate molecular O$_2$, copper catalysts have been applied to oxidation reactions like CO oxidation or propene epoxidation, with excellent results at the initial stages of the reaction.[19–27] However, the easy oxidation of metallic Cu^0 to cationic Cu$^+$ and Cu^{2+} always leads to a clear decay in activity and/or selectivity, revealing that it is necessary to avoid the formation of oxide phases under reaction conditions in order to maintain the catalytic performance constant. Despite this being a challenging goal, we demonstrated both theoretically and experimentally that it is possible to stabilize metallic Cu^0 under oxidizing reaction conditions by adjusting the size and shape of electrochemically synthesized Cu clusters.[28,29] The most stable isomers of the smallest Cu$_n$ clusters ($n \leq 5$) are planar and exhibit a resistance to oxidation that may be enough to overcome the problem. Larger clusters preferentially adopt a three-dimensional (3D) arrangement that promotes their oxidation in the presence of O$_2$ leading to very stable and less reactive adsorbed O atoms. Following this line of research, we recently investigated the mechanism of propene epoxidation on planar and 3D Cu$_5$ clusters, and confirmed the key role of cluster morphology in the selectivity to the epoxide.[30] Now, we extend this computational work to study the mechanism of CO oxidation, a prototypical reaction usually employed to explore the oxidation capabilities of potential catalysts. Since the key feature behind the different behaviour of the smallest Cu$_n$ clusters was traced to their morphology, both the planar and the 3D isomers of Cu$_5$ are considered, together with a larger 3D Cu$_8$ cluster to clarify the effect of both cluster size and shape on this reaction. The present study completes the description of CO oxidation on small Cu$_n$ clusters, including the work by Wang *et al.*[31] on Cu$_6$ and Cu$_7$, and other studies featuring icosahedral Cu$_{13}$,[32] Cu$_{20}$[33] and Cu$_{55}$.[34,35]

Results and discussion

Adsorption of CO and O$_2$ on Cu$_5$ and Cu$_8$ clusters

The adsorption of one molecule of carbon monoxide was studied on the two lowest isomers of Cu$_5$ (2D and 3D) and

Instituto de Tecnología Química, Universitat Politècnica de València – Consejo Superior de Investigaciones Científicas, Av de los Naranjos s/n, Valencia 46022, Spain. E-mail: boronat@itq.upv.es

Cu_8 (T_d and D_{2d}) in three possible adsorption modes, classified by the number of interactions between the carbon atom and the copper atoms: mono-coordinated on top of one Cu atom (*mono*), bi-coordinated on the edge between two copper atoms (*bridge*), and on the hollow site of a (111) facet, with the carbon atom bonded to three Cu atoms (*hcp*). A *mono* mode was obtained as preferential in all cases, with the bi-coordinated mode being stable only for Cu_5 clusters (Fig. 1a). Attempts to adsorb the CO in hollow sites always ended with the molecule being moved to another position. From Fig. 1, it can be seen that the interaction energies are somewhat stronger for Cu_5 than for Cu_8 clusters, consistent with previous studies,[36,37] with structure **4** of the Cu_5-3D isomer being especially stable. In addition, situations with higher CO coverage were considered for each cluster. Firstly, structures **10**, **12** and **14** (Fig. 1b) were built with one CO molecule per copper atom in the most stable *mono* mode. The corresponding structure for the Cu_8-D_{2d} isomer was not stable and evolved into structure **14**. Secondly, the maximum amount of CO molecules that each cluster can adsorb was investigated, leading to structures **11**, **13** and **15**. For planar Cu_5 clusters, the addition of more CO molecules produced a deformation of the cluster to the 3D isomer.

The addition of one CO molecule per copper atom averages the interaction energy on all available sites, better showing the overall interaction of the clusters with CO. Hence, the interaction is stronger for Cu_5-3D clusters, whereas planar Cu_5 shows the weakest interaction. The strong interaction of CO with the 3D isomer of Cu_5 can explain the deformation of the 2D isomer to the 3D one with the addition of even more CO molecules. As to the Cu_8-D_{2d} deformation, the very close energies of the two Cu_8 isomers, T_d and D_{2d}, allow their easy transformation into each other. Indeed, their coexistence was demonstrated experimentally by Lecoultre *et al.*,[38] and therefore a general 3D Cu_8 cluster without any specific symmetry is considered from now on in this study. Finally, comparison of structures **12** and **14** with **13** and **15**, respectively, shows that the addition of more CO molecules halves the average interaction energy, meaning that at least the last adsorption is not thermodynamically favoured.

The bonding of Cu_n clusters with CO is a result of two main interactions: the charge transferred from the HOMO of the molecule to the LUMO of the cluster and the back-bonding from the HOMO of the cluster to the anti-bonding $2\pi^*$ LUMO of the molecule. In addition to the energy of these orbitals, the strength of the interaction may depend on their shape and degeneracy, for a more fitting shape produces a better overlap. Due to all these, it is difficult to assess which property has the major contribution and determines the interaction. Nevertheless, the charge transferences described are favoured when the HOMO of the cluster is higher and its LUMO is lower in energy, and it can be seen that the order found for the adsorption energies (Cu_5-3D > Cu_5 > Cu_8) does indeed correlate qualitatively with the HOMO–LUMO gap found for these orbitals (Fig. 2). Indeed, the very stable structure **4** found for Cu_5-3D can be traced to the particular shape of the LUMO of the cluster: it has a large lobe at this adsorption site, so that the
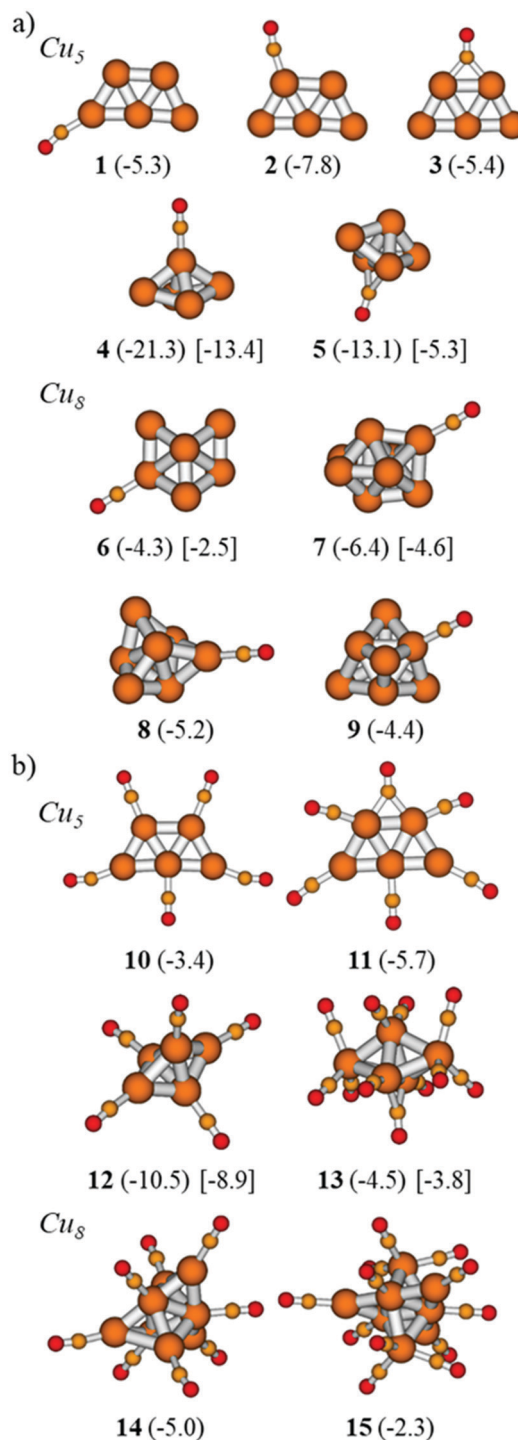

Fig. 1 Optimized structures for the adsorption of (a) one CO molecule and (b) more than one CO molecule in Cu_n clusters. Adsorption Gibbs energies in kcal mol^{-1} are indicated in parenthesis, averaged in the case of more than one CO. Values in brackets are calculated with respect to the most stable isomer per cluster size (Cu_5 planar and Cu_8-T_d).

overlap with the HOMO of the CO molecule is larger and the interaction is enhanced.

The interaction of O_2 with Cu_n clusters was thoroughly investigated in previous work.[28] The most stable systems

This journal is © the Owner Societies 2022

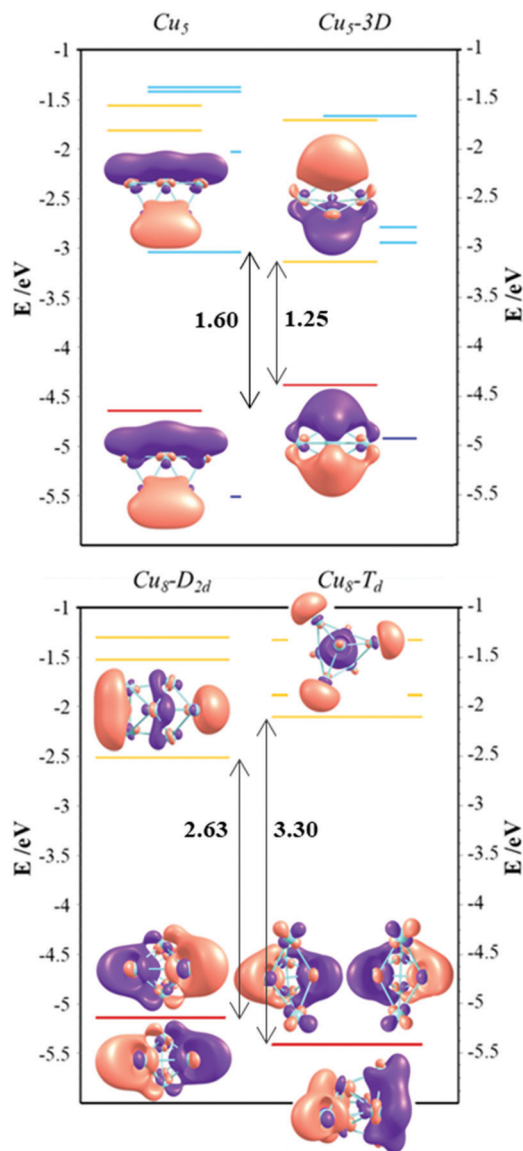*Phys. Chem. Chem. Phys.*, 2022, **24**, 4504–4514 | **4505**

Fig. 2 Stability (in eV) and composition of the highest occupied (HOMO) and lowest unoccupied (LUMO) molecular orbitals of Cu_n clusters (n = 5, 8) calculated at the B3PW91/6-311+G(d,p) level. HOMO−LUMO gap energy values are indicated with double ended arrows (in eV). Isosurface contour value: 0.03 e$^-$ Å^{-3}.
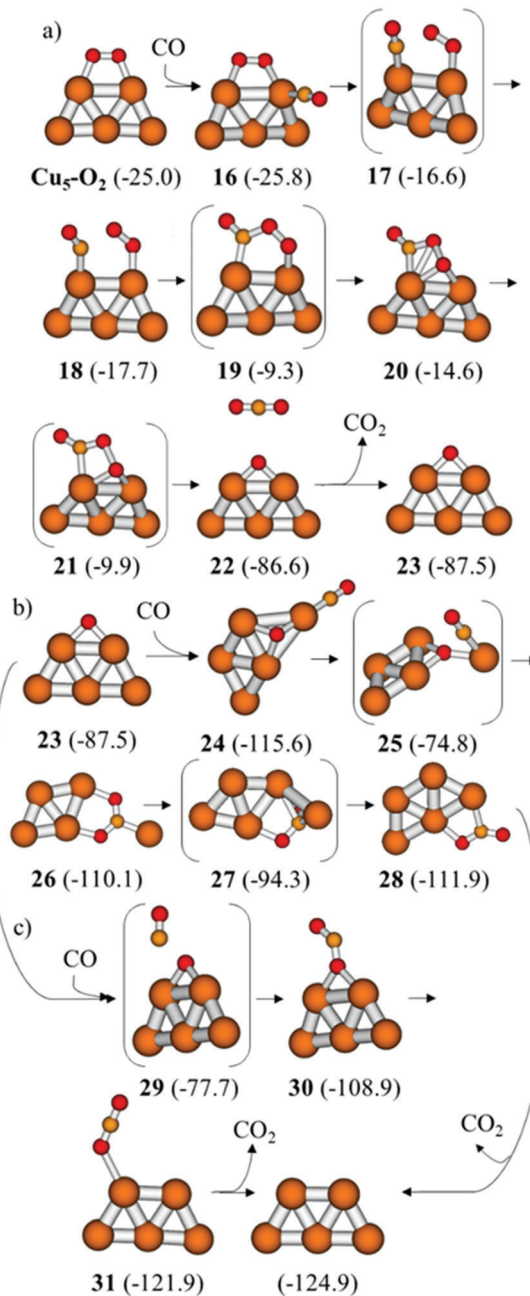

Fig. 3 Mechanism of CO oxidation by molecular O_2 on planar Cu_5, corresponding to the first (a) and the second (b and c) part of the catalytic cycle, respectively. Relative Gibbs energies (in kcal mol^{-1}) with respect to separate planar Cu_5 + O_2 + 2CO given in parenthesis. Cu in orange, C in amber, O in red. Energy profile in Fig. S1 (ESI†).

obtained for O_2 adsorbed on planar Cu_5, 3D Cu_5, and 3D Cu_8 clusters are structures **Cu5–O2, 3D-Cu5–O2** and **Cu8–O2** in Fig. 3–5, respectively, and their corresponding adsorption Gibbs energies are −25.0, −18.5 (−10.7 with respect to the planar isomer) and −3.3 kcal mol^{-1}. Therefore, for planar Cu_5 the interaction of the clusters with O_2 is always stronger than with CO, whereas for 3D Cu_5 they are similar, and for Cu_8 the interaction is similarly weak. With this in mind, we considered the co-adsorption of a CO molecule on the structures with O_2 already adsorbed just mentioned (Fig. 3–5). In addition, since the dissociation of O_2 on the 3D Cu_5 and Cu_8 clusters is easy (free activation energies of 15.8 and 14.9 kcal mol^{-1}, respectively),[28] the reaction mechanism starting with CO

adsorbed on a cluster with pre-dissociated O_2, *i.e.* with two oxygen atoms, was also studied. For planar Cu_5, however, the large Gibbs energy barrier involved in O_2 dissociation (40.1 kcal mol^{-1}) makes the reaction of CO with pre-dissociated O_2 unlikely and therefore it was not explored. On the other hand, several Langmuir–Hinshelwood (LH) or Eley–Rideal (ER) mechanisms can be stated for each system depending on whether the reactants are previously adsorbed (LH) or
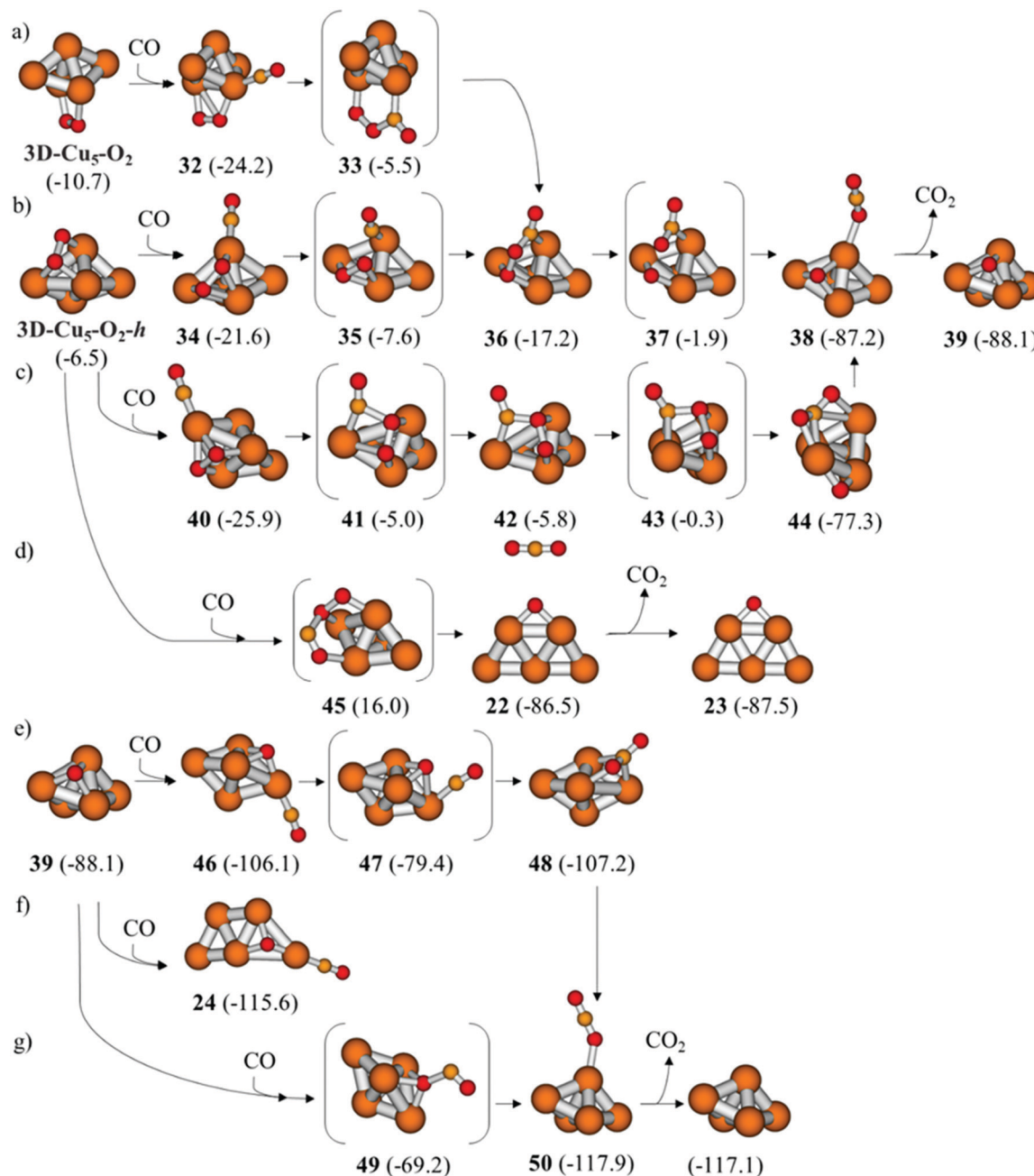
4506 | *Phys. Chem. Chem. Phys.*, 2022, **24**, 4504–4514

This journal is © the Owner Societies 2022

Fig. 4 Mechanism of CO oxidation by molecular O_2 on 3D Cu_5. (a–d) and (e–g) correspond to the first and second parts of the catalytic cycle, respectively. Relative Gibbs energies (in kcal mol^{-1}) with respect to separate planar Cu_5 + O_2 + 2CO given in parenthesis. Cu in orange, C in amber, O in red. Energy profile in Fig. S2 (ESI†).

one of them is not (ER). All these possibilities were computed and are described in detail below.

CO oxidation by molecular O_2 on planar Cu_5

Attempts to obtain an ER pathway from structure **Cu5–O2**, *i.e.* with the CO molecule coming from the gas phase, did not succeed. The reason is the low degree of activation of molecular O_2 in **Cu5–O2**, which makes the ER mechanism unlikely and explains the CO moving away or adsorbing on the cluster during the optimizations (Fig. 3a).

In structure **16**, the CO molecule adsorbs on the same copper atom where the oxygen is bonded with a very small adsorption energy. The approaching of CO to the O_2 molecule produces the breaking of one of the bonds that attached the latter to the cluster, which can be seen at the imaginary frequency of -100 cm^{-1} that characterizes transition state **17**, and ultimately leads to intermediate **18**, where both molecules are mono-coordinated to copper and closer to each other. This first step has an activation energy of 9.2 kcal mol^{-1}. The free oxygen atom of the O_2 molecule binds then to the close carbon
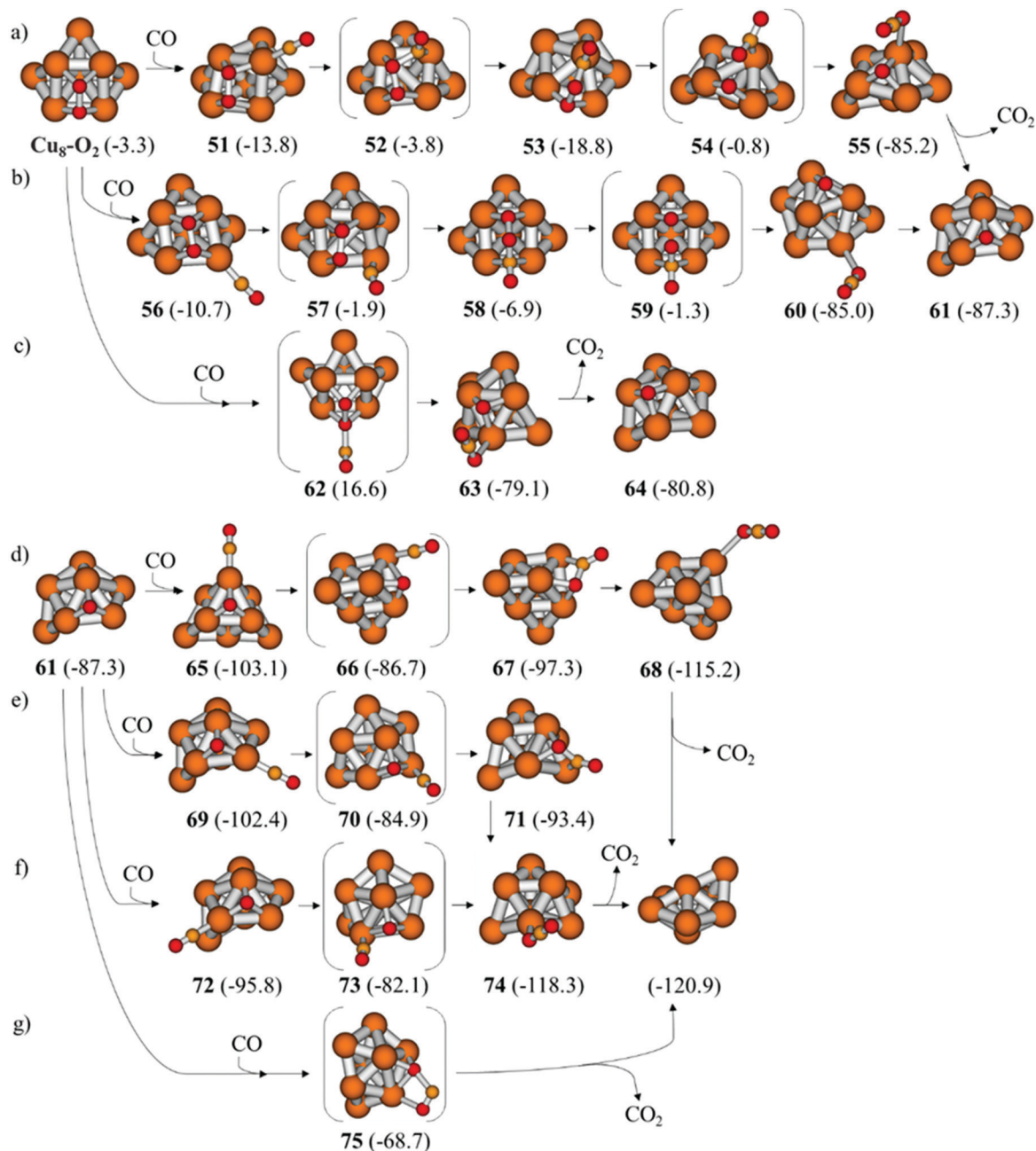
Fig. 5 Mechanism of CO oxidation by molecular O_2 on 3D Cu_8. (a–c) and (d–g) correspond to the first and second parts of the catalytic cycle, respectively. Relative Gibbs energies (in kcal mol^{-1}) with respect to separate Cu_8-T_d + O_2 + $2CO$ given in parenthesis. Cu in orange, C in amber, O in red. Energy profile in Fig. S4 (ESI†).

atom of the CO molecule in a process that requires another 8.4 kcal mol^{-1} (TS **19**) and produces the OOCO species **20** as an intermediate.

From here, the dissociation of the oxygen molecule through TS **21** is easy, leading to the formation of a CO_2 molecule with an activation energy of only 4.7 kcal mol^{-1} in a very exothermic process (ΔG_{reac} = −72.0 kcal mol^{-1}) and leaving the cluster with an oxygen atom adsorbed in an edge mode, as can be seen in products **22** and **23**. In order to close the catalytic cycle, the reaction of structure **23** with a second CO molecule was studied

(Fig. 3b). Its adsorption on the site close to the oxygen atom produces structure **24**, with an oxygen atom within the cluster, almost separating one copper atom from the rest. This type of oxidized structure has also been reported for planar Cu_6.[31] From **24**, the reaction would imply a 40.8 kcal mol^{-1} barrier and a thermodynamically unfavoured product where the cluster is broken into planar rhombic Cu_4 + Cu_1, which are bridged by the CO_2 formed (structure **26**). The Cu_5 cluster can be recovered with a barrier of 15.8 kcal mol^{-1} (structure **27**) and produces an unfavourably adsorbed bent CO_2 that readily desorbs (structure

28). Fig. 3c shows instead a much more favourable ER mechanism. Indeed, the direct reaction of atomic O with gas-phase CO through TS **29** requires only 9.8 kcal mol^{-1} of energy. The CO_2 produced is adsorbed through one of the oxygen atoms in a bi-coordinated mode (structure **30**), but it is more stable mono-coordinated (structure **31**) and also desorbs favourably, leaving the planar cluster naked again. Therefore, catalysis of the CO oxidation by O_2 on planar Cu_5 clusters is possible. It is found that CO, much like water,[29] facilitates the dissociation of O_2, lowering the energy from the high 40.1 kcal mol^{-1} of the monomolecular reaction to the 4.7 kcal mol^{-1} of step **20-[21]-22**. More importantly, although the O_2 molecule readily dissociates producing CO_2, the remaining O atom on an edge reacts easily as well. However, the adsorption of CO in this structure is strong (28.1 kcal mol^{-1}) and leads to a stable oxidized structure (**24**) that can deactivate the catalyst.

CO oxidation by molecular O_2 on 3D Cu_5

The individual steps for the LH path on 3D Cu_5 (Fig. 4a) are similar to those on planar Cu_5 (Fig. 3a), first producing an OOCO intermediate to subsequently break its O–O bond. However, the reactions take place in the *h*-111 facet of the 3D cluster as opposed to the edge of the planar Cu_5.

Indeed, although we initially started from structure **3D-Cu5–O2**, the first step of the reaction led to structure **36**, where the OOCO intermediate is bent in order to occupy this *h*-111 facet (Fig. 4a). Consequently and in line with the previous O_2 dissociation studied, we also included structure **3D-Cu5–O2-h** in this study, which gave rise to two LH mechanisms (Fig. 4b and c). CO can adsorb on structure **3D-Cu5–O2-h** in two different sites near the O_2 molecule with similar adsorption energies, leading to structures **34** and **40**. Then, activation energies of 14.0 and 20.5 kcal mol^{-1}, respectively, are obtained to produce intermediate OOCO species **36** and **42**. Finally, the dissociation of the O_2 molecule producing CO_2 through the corresponding TSs **37** and **43** involve barriers of 15.3 and 5.5 kcal mol^{-1}, respectively. The CO_2 formed in the second LH case (Fig. 4c) is first stabilized in a bent geometry, with each oxygen bonded to a Cu atom and the carbon establishing three bonds with the copper atoms nearby (structure **44**). A similar structure involving a CO_2 adsorbed in a bent position has already been reported for copper clusters of 7 and 13 atoms.[39] It can evolve to the same more stable mono-coordinated mode that is directly obtained in the first LH case (Fig. 4b, structure **38**), and again it desorbs a bit favourably, easily leaving the cluster with an oxygen atom adsorbed in an *hcp* facet (structure **39**).

Again, no ER mechanism was found for O_2 adsorbed in a *bridge* mode in structure **3D-Cu5–O2**, whereas from structure **3D-Cu5–O2-h** a direct mechanism involving a somewhat higher barrier (22.5 kcal mol^{-1}) was found (Fig. 4d). Through TS **45**, where the CO molecule coordinates through its oxygen atom to the cluster, the formation of CO_2 occurs, but also the deformation of the cluster again into its planar isomer occurs, with an oxygen atom adsorbed in an edge mode, *i.e.* the same structure **23** that was found in the LH case for planar Cu_5. As a result, in this case the cycle is closed through the path shown in Fig. 3c, with a 9.8 kcal mol^{-1} barrier only. For the other two paths,

however, the possible LH and ER mechanisms from structure **39** must be considered. Adsorption of CO on the site with the highest coordination produces structure **24** again, from which the reaction is unlikely (Fig. 4f and Fig. S2, ESI†). The adsorption on the less coordinated Cu produces structure **46**, 9.5 kcal mol^{-1} higher in energy than **24**, which requires 26.7 kcal mol^{-1} of energy to produce a bent CO_2 (Fig. 4e). As in the other cases where a bent CO_2 was obtained, it can evolve to a more stable mono-coordinated mode (structure **50**) and in this case desorbs with a very small energy cost of 0.8 kcal mol^{-1}. In contrast, the direct ER pathway requires 18.9 kcal mol^{-1} of energy to produce the same structure **50** with CO_2 in a *mono* mode through TS **49** (Fig. 4g).

To sum up, for 3D Cu_5 it is found that the CO + O_2 (LH) reaction competes with the O_2 dissociation, with individual steps in the 14–20 kcal mol^{-1} range (*vs.* 15.8 kcal mol^{-1} for monomolecular O_2 dissociation). The ER mechanism is also possible with a slightly higher activation energy (22.5 kcal mol^{-1}), and it produces again the planar cluster whose bi-coordinated O atom reacts easily (9.8 kcal mol^{-1}), but on which the adsorption of CO may deactivate the catalyst. The easier LH paths mentioned leave the cluster with a three-coordinated O atom that requires almost twice as much energy to react with CO (18.9 kcal mol^{-1}), and it does so also through an ER mechanism. The possible deactivation in the second part of the cycle for both isomers seems to be caused by the increased adsorption energy of CO at the more oxidized clusters and by the stability of the resulting structures **24** and **46**. In this situation, more CO molecules may adsorb on the cluster, and such adsorption may draw the O atom closer to one of them, decreasing the energy barrier required for them to react. Indeed, it was found that the addition of more CO molecules is thermodynamically favoured and decreases the activation energy for both isomers, from 40.8 to 21.7 kcal mol^{-1} in planar Cu_5 and from 26.7 to 9.7 kcal mol^{-1} in 3D Cu_5 (Fig. S3, ESI†). Consequently, deactivation of the catalyst from structures such as **24** and **46** is not definitive and it may not be an issue. Notice, however, that structure **S5** recovers a 3D Cu_5 geometry instead of a planar one, driven by the CO molecule remaining. Thus, as observed in the adsorption section, the presence of a higher concentration of CO may favour the 3D isomer of Cu_5 over the planar one.

CO oxidation by molecular O_2 on 3D Cu_8

Again, as depicted in Fig. 5, the reaction mechanisms found are similar to those obtained for the Cu_5 clusters, with a few exceptions. Firstly, in the path shown in Fig. 5b, the OOCO intermediate is stabilized on a (100) facet (structure **58**) which is not possible in Cu_5. We find again a somewhat higher activation on this mode with respect to that on a (111) facet (the O–O bond distance increases from 1.44 Å in structure **53** to 1.46 Å in **58**) and a lower activation energy for the O–O bond breaking steps (5.6 *vs.* 18.0 kcal mol^{-1}). However, in those minima the O_2 is equally three-coordinated, and this difference in the activation energies seems to be caused by the increased stabilization of the OOCO intermediate on the (111) facet,

This journal is © the Owner Societies 2022

Phys. Chem. Chem. Phys., 2022, **24**, 4504–4514 | **4509**

structure **53**, with respect to structure **58**. The reason is probably that the C atom is three-coordinated instead of tetra-coordinated and can preserve a double-bond nature in the C–O interaction with the uncoordinated O atom. Regarding the ER path, we find that it is again a bit higher in energy with respect to LH mechanisms (19.9 *vs.* 18.0/8.8 kcal mol^{-1}), although it is a bit lower compared to the ER pathway of 3D Cu_5, consistent with the more activated O_2 molecule in structure **Cu8–O2**. To close the cycle, the ER path is very similar to the one on 3D Cu_5 but with the CO coordinating with its O, and the activation energy is also similar, 18.6 kcal mol^{-1} (Fig. 5g), showing that the three-coordinated O atom is equally stable on 3D Cu_5 and Cu_8. However, the barriers for the LH paths for Cu_8 are lower than those for the ER mechanism and consequently lower than those for the LH paths of 3D Cu_5 (16.4/17.5 *vs.* 26.7 kcal mol^{-1}). The latter is likely due to the fact that 3D Cu_5 stabilizes CO in a position at which it is much more separated from the O atom. As seen before, adding two more CO molecules to structure **46**, thus forcing the former CO to move closer, decreases the energy barrier to 9.6 kcal mol^{-1} (Fig. S3, ESI†). Altogether, we find that the bimolecular reaction between adsorbed O_2 and CO is possible for the three clusters. No ER mechanism was found on planar Cu_5, possibly because the lower activation of the O_2 molecule renders it costly. In contrast, barriers within the LH and ER pathways are comparable for 3D Cu_5 and Cu_8, still being slightly lower for LH mechanisms. Moreover, the activation energy for the ER reaction is a bit lower for Cu_8, consistent with the O_2 molecule being more activated at it. Then, removing the O atom from the clusters to close the cycle is easiest for the edge-stabilized O atoms on planar Cu_5, whereas on Cu_8 and 3D Cu_5 it requires twice as much energy. For both Cu_5 isomers, the ER pathway is preferred for this last step, whereas for Cu_8 the LH path is slightly easier. The rate-determining step for planar Cu_5 is the formation of the first CO_2, more specifically the formation of the OOCO intermediate, whereas for 3D Cu_5 and Cu_8 the two parts of the cycle have comparable barriers.

CO oxidation by dissociated O_2 on 3D Cu_5 ($Cu_5(O)_2$)

As depicted in Fig. 6, adsorption of the CO molecule at two of the three inequivalent sites close to the O atoms of structure **Cu5(O)2**, which comes from the dissociation of O_2 on 3D Cu_5, deforms the cluster into a structure similar to **24** with an additional O atom adsorbed on an edge (structure **76**). From this intermediate, the reaction follows a similarly costly path towards CO_2 formation (Fig. 6a). For the third one, at the Cu atom coordinated to both O atoms, the cluster deforms again, but to adopt the more stable geometry already seen after the dissociation of O_2 in the planar cluster (structure **81**). From here, the formation of CO_2 requires 15.7 kcal mol^{-1} of energy and produces through TS **82** the molecule in a bent geometry on a (111) facet again (structure **83**). As before, the molecule is more stable mono-coordinated and deforms back to 3D Cu_5 (structure **36**), hence desorbing a bit favourably (-0.9 kcal mol^{-1}).
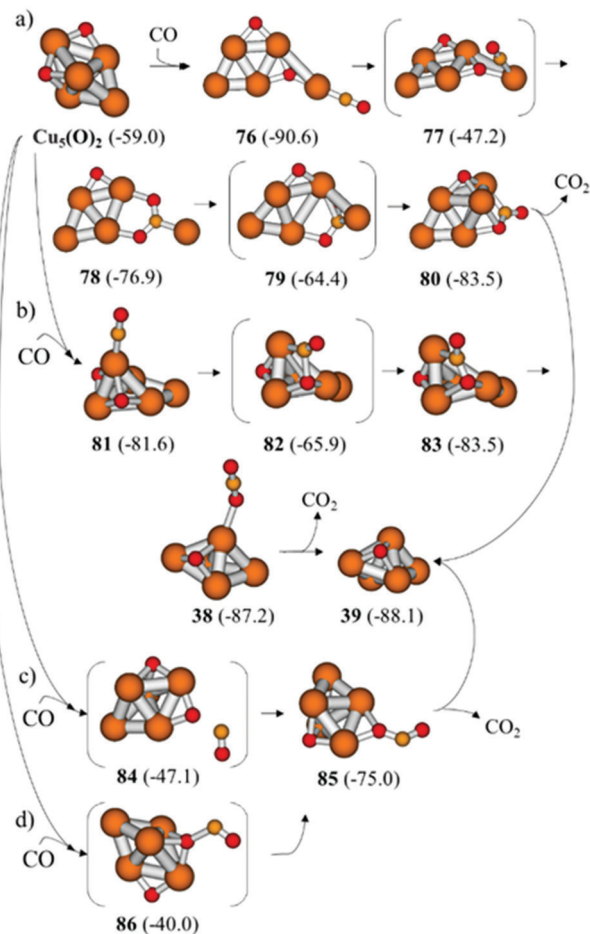

Fig. 6 Mechanism of CO oxidation by dissociated O_2 on 3D Cu_5. Relative Gibbs energies (in kcal mol^{-1}) with respect to separate planar Cu_5 + O_2 + 2CO given in parenthesis. Cu in orange, C in amber, O in red. Energy profile in Fig. S5 (ESI†).

Regarding ER pathways, regardless of whether the CO reacts with the O in the edge position (TS **84**) or with the three-coordinated one (TS **86**), the cluster ends accommodating the resulting CO_2 in a bi-coordinated adsorption mode on an edge (structure **85**). However, the difference between the two O atoms is observed in TS structures **84** and **86** and in their corresponding activation energies, 7.1 kcal mol^{-1} lower for the one with the less stable O atom adsorbed on the edge (Fig. 6c and d). Desorption of CO_2 produces always the 3D Cu_5 cluster with a three-coordinated O atom seen before (structure **39**), and therefore closing the cycle would be accomplished *via* the path shown in Fig. 4e–g.

To summarize, there is not a big difference between LH and ER barriers for the reaction of CO with atomic oxygen when there is one or two O atoms, although the barrier for the 81-[82]-83 LH path is noticeably lower (*vs.* the 46-[47]-48 path in Fig. 4), probably due to the reactants being closer. Besides, these $[(O)O\cdots CO]^{\neq}$ ER barriers suggest that removing the first O atom from Cu_5 is somewhat easier than removing the second one ($[O\cdots CO]^{\neq}$) due to one of them being only bi-coordinated. However, since structure **Cu5(O)2** easily evolves to a cluster with

4510 | *Phys. Chem. Chem. Phys.*, 2022, **24**, 4504–4514

This journal is © the Owner Societies 2022

three-coordinated O atoms that react more difficultly, this difference may not be observable. Finally, the cluster may suffer deactivation due to the formation of structure **76** but, again, it was found that barriers decrease if a second CO molecule is adsorbed (Fig. S6, ESI†).

CO oxidation by dissociated O_2 on 3D Cu_8 ($Cu_8(O)_2$)

In structure **Cu8(O)2** in Fig. 7 there are two inequivalent adsorption sites close to the O atoms that lead to structures **87** and **91** and their respective LH paths, which involve similar barriers of 4.7 and 3.9 kcal mol^{-1} to produce the first CO_2. The latter is in a bent position over a (111) facet (structures **89** and **93**) prior to its favourable desorption. These barriers are significantly lower than the ones found in the previous section,

even for the second part of the cycle with atomic O. The ER path involves a much higher barrier of 21.5 kcal mol^{-1}, again showing that the three-coordinated O atoms are as stable as those on Cu_5 3D (Fig. 6d), with the 2.5 kcal mol^{-1} activation energy increase being likely due to the more linear O–Cu–O stable bond formed in structure **Cu8(O)2**, which is not as good in structure **Cu5(O)2**.

After CO_2 desorption, the cluster remains in the geometry observed in **Cu8(O)2** (structure **90**), instead of recovering structure **61**, and therefore the closing of the cycle was also studied from structure **90**. However, the adsorption of a CO molecule close to the O atom leads to structures **65** and **69** found previously (Fig. 5d and e), and the ER path found has a 18.0 kcal mol^{-1} activation energy (Fig. 7f), very similar to what was obtained from structure **61** (19.9 kcal mol^{-1}, Fig. 5g).

O_2 dissociation in the presence of co-adsorbed CO

For 3D Cu_5 and Cu_8 clusters, the bimolecular reaction with CO competes with the monomolecular O_2 dissociation. The differences are not large and might be compensated by the adsorption of CO, which is larger for 3D Cu_5 and may induce the bimolecular reaction. However, calculating the dissociation of O_2 in the presence of one co-adsorbed CO molecule yields barriers somewhat lower than the lone monomolecular dissociation for the most stable adsorptions (Fig. 8), thus supporting the monomolecular O_2 dissociation as the first step of the mechanism. These results are thus consistent with the work of Wang *et al.*[31] on Cu_6 and Cu_7 clusters, where the best paths show transition states where the CO molecule stays far from O_2 and practically does not participate in the rupture of the O–O bond.

Note that although the authors start the study with the most stable planar Cu_6 isomer, O_2 adsorption deforms the cluster into a 3D structure upon which the molecule adsorbs in an *h*-111 mode. This deformation into 3D morphology was also observed in our first study[28] and explains the resulting similarity between Cu_6 and 3D Cu_5, Cu_7 and Cu_8 in the first part of the catalytic CO oxidation cycle. Given that O_2 dissociation is increasingly favoured with increasing size, it is coherent that larger particles also favour the initial O_2 dissociation over the LH bimolecular reaction with CO.[32–35] This is consistent with our previous statement that morphology brings the more significant changes and the results on Cu_{5-8} clusters show that the differential reactivity is rapidly lost with increasing size as soon as the *h*-111 and *h*-100 facets become available. Indeed, the available reports on larger particles show that the second part of the cycle occurs *via* a LH mechanism in which the rate determining step is the O + CO reaction, which means that the whole reaction for Cu_8 is already qualitatively equivalent to that of larger clusters, namely, Cu_{13},[32] Cu_{20}[33] and Cu_{55}.[34,35]

Therefore, our calculations indicate that for both 3D Cu_5 and Cu_8 clusters the predominant mechanism starts with the monomolecular dissociation of O_2 (11.7 and 13.7 kcal mol^{-1} of activation energies, respectively), followed by the LH step of the formation of the first CO_2 molecule (15.7 and 4.7 kcal mol^{-1}), and finally by the formation of the second CO_2 molecule
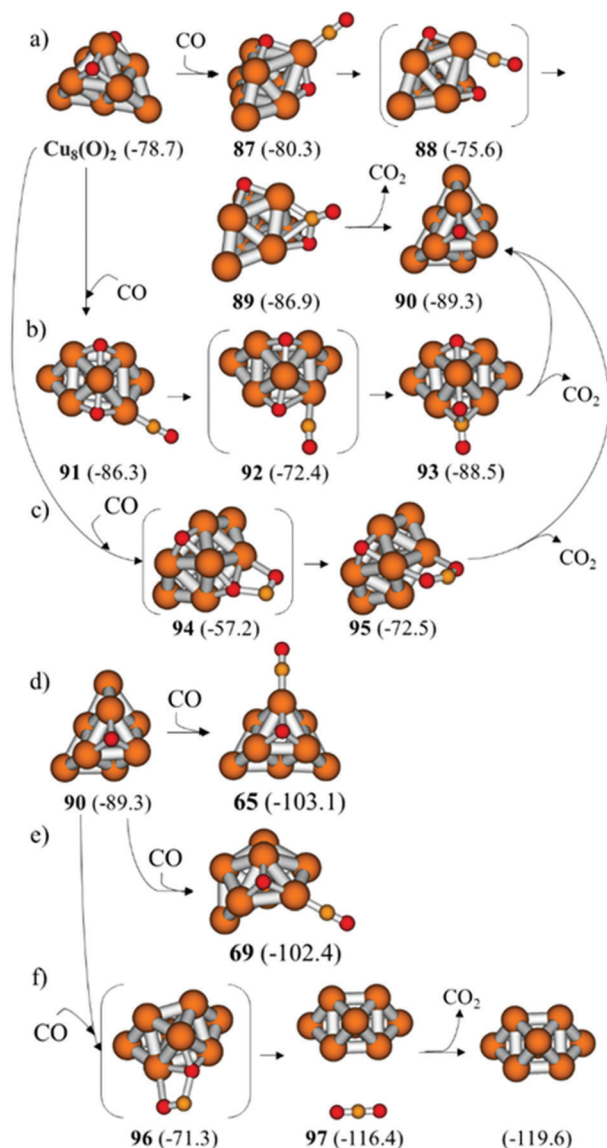

Fig. 7 Mechanism for CO oxidation by dissociated O_2 on 3D Cu_8. Relative Gibbs energies (in kcal mol^{-1}) with respect to separate Cu_8-T_d + O_2 + 2CO given in parenthesis. Cu in orange, C in amber, O in red. Energy profile in Fig. S7 (ESI†).

This journal is © the Owner Societies 2022

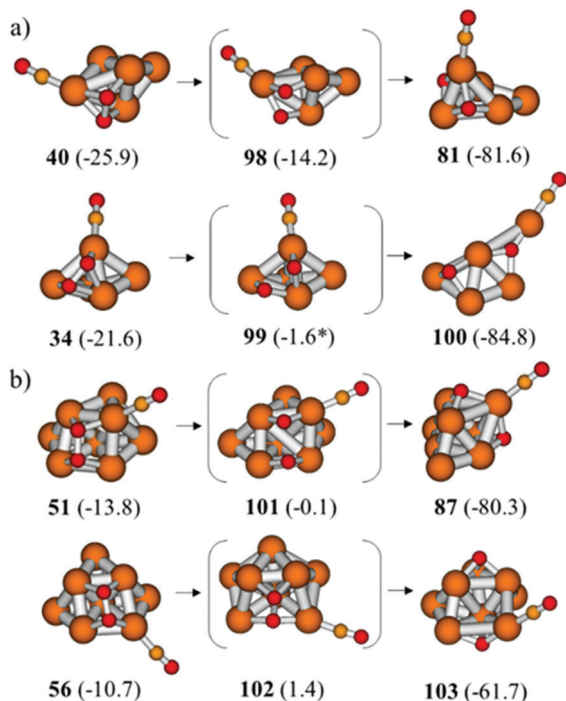*Phys. Chem. Chem. Phys.*, 2022, **24**, 4504–4514 | **4511**

Fig. 8 Optimized structures for the monomolecular dissociation of O_2 with co-adsorbed CO in (a) 3D Cu_5 and (b) Cu_8. Relative Gibbs energies with respect to separate planar Cu_5 + O_2 + 2CO and Cu_8 + O_2 + 2CO, respectively, given in parenthesis in kcal mol^{-1}. Cu in orange, C in amber, O in red. The cluster was fixed during optimization of structure **99**, as it otherwise evolved to **100**.
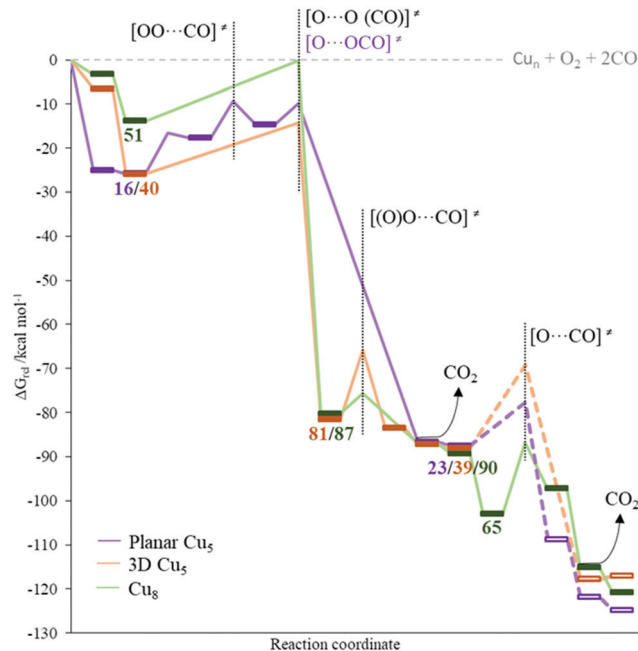

Fig. 9 Energy profile of the best mechanisms found for the catalytic CO oxidation by planar Cu_5, 3D Cu_5 and 3D Cu_8 clusters. Dashed lines correspond to ER paths. Key transition states indicated by vertical lines.

(18.9 and 16.4 kcal mol^{-1}), with the difference that the latter is a LH step for Cu_8, because, as mentioned, the CO is closer to the O atom than for 3D Cu_5, for which the ER step has a lower barrier (Fig. 9).

Note that the data presented suggest that planar clusters may only keep their geometry if the concentration or partial pressure of CO is low during the reaction. Otherwise, they are likely to deform into 3D clusters. However, the results also indicate that the latter will only be slightly worse for the catalysis of CO oxidation: for planar clusters the formation of the OOCO intermediate will be the rate determining step of the reaction (16.5 kcal mol^{-1}), whereas for 3D clusters the predominant mechanism just mentioned has an activation energy for the rate determining step of 18.9 kcal mol^{-1}. Furthermore, the presence of a higher concentration of CO may avoid the deactivation of Cu_5 clusters due to structures with the O atoms between copper atoms because the CO molecules get closer to the latter facilitating their reaction. Besides, according to the predominant mechanism, Cu_8 would represent a similar or even slightly better candidate (a rate determining step barrier of 16.4 kcal mol^{-1}), but the predominance of the path is lower (the highest activation energy of other paths that contribute is 18.0 kcal mol^{-1}). More importantly, according to the easier oxidation and larger resistance to reduction observed for the Cu_8 sample in our previous work,[29] it is likely to oxidize to a larger extent than considered in these calculations due to, for

instance, subsequent oxidation reactions at other available facets of the Cu_8 cluster. To determine whether such oxidation would be enough to deactivate the catalyst would require further study, because small $Cu_{12}O_x$ oxidized clusters have recently shown enhanced catalytic activity in the C–H oxidation of methyl aromatic compounds, for instance,[40] and another study reports that partially oxidized icosahedral $Cu_{55}(O)_{40}$ does not lose its catalytic activity towards CO oxidation, suggesting that it may not deactivate even when fully oxidized.[35]

Experimental

All calculations in this work are based on density functional theory (DFT) and were carried out using the Gaussian 09 program package.[41] The B3PW91 functional was employed, which combines the PW91 correlation functional by Perdew and Wang with Becke's hybrid three-parameter exchange functional.[42–44] Since the Def2TZVP[45,46] basis set shows a very good performance at an affordable cost for Cu,[28] it was used for Cu atoms, whereas the standard 6-311+G(d,p) basis set by Pople was employed for the rest.[47] Regarding multiplicity, Cu_5 structures, guided by previous studies,[28,29,36,37] were always calculated as doublet states, whereas for Cu_8 structures triplet states were explored, in all cases becoming more unstable than their singlet counterparts. The default unrestricted formalism of Gaussian was automatically applied for structures with multiplicities higher than singlet. In all cases, the positions of all atoms in each system were fully optimized without any restriction, and all stationary points were characterized by pertinent frequency analysis calculations. Transition states were

determined through potential energy surface (PES) scans along with the subsequent optimizations and vibrational frequency calculations. Atomic charges and molecular orbital distributions were calculated using the natural bond orbital (NBO) approach.[48]

Conclusions

All clusters investigated, namely, planar Cu_5, 3D Cu_5 and 3D Cu_8, are able to catalyze the CO oxidation reaction. The highest activation energy among the steps of the lowest energy pathway is similar for the three of them and is about 16–18 kcal mol^{-1}. There are, however, clear differences in the reaction mechanism associated to cluster morphology rather than to cluster size.

On the two 3D clusters, Cu_5 and Cu_8, the O_2 molecule dissociates first, even in the presence of adsorbed CO, and then two CO molecules react with the resulting O atoms. LH mechanisms are favoured on Cu_8 for both CO + O steps, with the first being significantly easier. On 3D Cu_5, a LH mechanism is still preferential for the first CO + O step, although with a higher activation energy due to the molecule being far from the O atom, but for the second the ER mechanism is a bit easier. In both of them, the second CO + O step is the rate determining step. In contrast, planar Cu_5 did not catalyse O_2 dissociation well, and thus the reaction proceeds through formation of an OOCO intermediate, whose O–O bond is broken in a second step releasing the first CO_2 and leaving one adsorbed O atom. The latter is bi-coordinately adsorbed, which lowers the activation energy needed for the final CO + O ER step. As a result, the rate determining step of the reaction is the formation of the OOCO intermediate.

Planar Cu_5 seems to be prone to deformation towards 3D Cu_5 with a high pressure of CO, but such an effect would not diminish the catalytic activity of Cu_5 clusters. In some cases, however, structures where an O atom gets inserted into the Cu_5 cluster structure have been obtained, for which further reaction gets complicated, increasing the activation energy of some steps. Nevertheless, the presence of other CO molecules has proven to be enough to put the O atom nearer to a CO and recover low barriers. On the other hand, subsequent oxidation reactions at other available facets of the Cu_8 cluster are likely to oxidize Cu_8 to a larger extent, possibly diminishing its catalytic activity.

The results obtained are consistent with previous reports on copper particles of different sizes and at the same time provide a more complete account of the behaviour of the smallest copper clusters, showing again that presenting a planar or a 3D morphology produces the most significant changes to the catalytic behaviour of these subnanometric systems, even though it does not translate into a substantial difference in catalytic activity in this specific reaction.

Author contributions

M. B. and A. C. directed the study. E. F. carried out the DFT calculations. All the authors discussed the results and contributed to the preparation, writing and revision of the manuscript.

Conflicts of interest

There are no conflicts to declare.

Acknowledgements

Notes and references

1 M. Boronat, A. Leyva-Pérez and A. Corma, *Acc. Chem. Res.*, 2014, **47**, 834.
2 E. C. Tyo and S. Vajda, *Nat. Nanotechnol.*, 2015, **10**, 577.
3 L. Liu and A. Corma, *Chem. Rev.*, 2018, **118**, 4981.
4 X. Liu and D. Astruc, *Coord. Chem. Rev.*, 2018, **359**, 112.
5 J. Yan, B. K. Teo and N. Zheng, *Acc. Chem. Res.*, 2018, **51**, 3084.
6 K. Yamamoto, T. Imaoka, M. Tanabe and T. Kambe, *Chem. Rev.*, 2019, **120**, 1397.
7 E. Fernández and M. Boronat, *J. Phys.: Condens. Matter*, 2019, **31**, 013002.
8 C. Dong, Y. Li, D. Cheng, M. Zhang, J. Liu, Y. G. Wang, D. Xiao and D. Ma, *ACS Catal.*, 2020, **10**, 11011.
9 S. Maola and H. Häkkinen, *Nat. Commun.*, 2021, **12**, 2197.
10 H. Rong, S. Ji, J. Zhang, D. Wang and Y. Li, *Nat. Commun.*, 2021, **11**, 5884.
11 J. Oliver-Meseguer, J. R. Cabrero-Antonino, I. Dominguez, A. Leyva-Perez and A. Corma, *Science*, 2012, **338**, 1452.
12 A. Corma, P. Concepcion, M. Boronat, M. J. Sabater, J. Navas, M. J. Yacaman, E. Larios, A. Posadas, M. A. Lopez-Quintela, D. Buceta, E. Mendoza, G. Guilera and A. Mayoral, *Nat. Chem.*, 2013, **5**, 775.
13 L. Lei, F. Mehmood, S. Lee, J. Greeley, B. Lee, S. Seifert, R. E. Winans, J. W. Elam, R. J. Meyer, P. C. Redfern, D. Teschner, R. Schlögl, M. J. Pellin, L. A. Curtiss and S. Vajda, *Science*, 2010, **328**, 224.
14 W. E. Kaden, T. Wu, W. A. Kunkel and S. L. Anderson, *Science*, 2009, **326**, 826.
15 E. Fernández, M. A. Rivero-Crespo, I. Domínguez, P. Rubio-Marqués, J. Oliver-Meseguer, L. Liu, M. Cabrero-Antonino, R. Gavara, J. C. Hernández-Garrido, M. Boronat, A. Leyva-Pérez and A. Corma, *J. Am. Chem. Soc.*, 2019, **141**, 1928.
16 F. Garnes-Portolés, R. Greco, J. Oliver-Meseguer, J. Castellanos-Soriano, M. C. Jiménez, M. López-Haro, J. C. Hernández-Garrido, M. Boronat, R. Pérez-Ruiz and A. Leyva-Pérez, *Nat. Catal.*, 2021, **4**, 293.
17 L. Liu, D. N. Zakharov, R. Arenal, P. Concepcion, E. A. Stach and A. Corma, *Nat. Commun.*, 2018, **9**, 574.

This journal is © the Owner Societies 2022

Phys. Chem. Chem. Phys., 2022, **24**, 4504–4514 | **4513**

18 P. Serna, A. Rodríguez-Fernández, S. Yacob, C. Kliewer, M. Moliner and A. Corma, *Angew. Chem., Int. Ed.*, 2021, **60**, 15954.

19 S. Royer and D. Duprez, *ChemCatChem*, 2011, **3**, 24.

20 G. G. Jernigan and G. A. Somorjai, *J. Catal.*, 1994, **147**, 567.

21 V. A. Sadykov, S. F. Tikhov, N. N. Bulgakov and A. P. Gerasev, *Catal. Today*, 2009, **144**, 324.

22 Sd F. Xu, K. Mudiyanselage, A. E. Baber, M. Soldemo, J. Weissenrieder, M. G. White and D. J. Stacchiola, *J. Phys. Chem. C*, 2014, **118**, 15902.

23 B. Eren, C. Heine, H. Bluhm, G. A. Somorjai and M. Salmeron, *J. Am. Chem. Soc.*, 2015, **137**, 11186.

24 A. Marimuthu, J. Zhang and S. Linic, *Science*, 2013, **339**, 1590.

25 Q. Hua, T. Cao, X. K. Gu, J. Lu, Z. Jiang, X. Pan, L. Luo, W. X. Li and W. Huang, *Angew. Chem., Int. Ed.*, 2014, **53**, 4856.

26 Y. Y. Song, B. Dong, S. W. Wang, Z. R. Wang, M. Zhang, P. Tian, G. C. Wang and Z. Zhao, *ACS Omega*, 2020, **5**, 6260.

27 T. T. Xiao, R. S. Li and G. C. Wang, *J. Phys. Chem. C*, 2020, **124**, 6611.

28 E. Fernandez, M. Boronat and A. Corma, *J. Phys. Chem. C*, 2015, **119**, 19832.

29 P. Concepcion, M. Boronat, S. Garcia-Garcia, E. Fernandez and A. Corma, *ACS Catal.*, 2017, **7**, 3560.

30 E. Fernandez, M. Boronat and A. Corma, *J. Phys. Chem. C*, 2020, **124**, 21549.

31 Y. Wang, G. Wu, M. Yang and J. Wang, *J. Phys. Chem. C*, 2013, **117**, 8767.

32 T. T. Li, C. He, W. X. Zhang and M. Cheng, *Appl. Surf. Sci.*, 2019, **479**, 39.

33 L. Ma, M. Melander, K. Laasonen and J. Akola, *Phys. Chem. Chem. Phys.*, 2015, **17**, 7067.

34 D. Tang and J. Zhang, *RSC Adv.*, 2013, **3**, 15225.

35 L. Ma and J. Akola, *Phys. Chem. Chem. Phys.*, 2019, **21**, 11351.

36 A. Poater, M. Duran, P. Jaque, A. Toro-Labbe and M. Sola, *J. Phys. Chem. B*, 2006, **110**, 6526.

37 L. Padilla-Campos, *J. Mol. Struct.: THEOCHEM*, 2008, **851**, 15.

38 A. Rydlo, C. Felix, J. Buttet, S. Gilb and W. Harbich, *J. Chem. Phys.*, 2011, **134**, 074303.

39 S. Gautam, K. Dharamvir and N. Goel, *Comput. Theor. Chem.*, 2013, **1009**, 8.

40 K. Sonobe, M. Tanabe and K. Yamamoto, *ACS Nano*, 2020, **14**, 1804.

41 M. J. Frisch; G. W. Trucks; H. B. Schlegel; G. E. Scuseria; M. A. Robb; J. R. Cheeseman; G. Scalmani; V. Barone; B. Mennucci and G. A. Petersson *et al. Gaussian 09, Revision C.01*, Gaussian, Inc., *Wallingford CT*, 2009.

42 A. D. Becke, *J. Chem. Phys.*, 1993, **98**, 5648.

43 J. P. Perdew, J. A. Chevary, S. H. Vosko, K. A. Jackson, M. R. Pederson, D. J. Singh and C. Fiolhais, *Phys. Rev. B: Condens. Matter Mater. Phys.*, 1992, **46**, 6671.

44 J. P. Perdew and Y. Wang, *Phys. Rev. B: Condens. Matter Mater. Phys.*, 1992, **45**, 13244.

45 F. Weigend and R. Ahlrichs, *Phys. Chem. Chem. Phys.*, 2005, **7**, 3297.

46 F. Weigend, *Phys. Chem. Chem. Phys.*, 2006, **8**, 1057.

47 J. S. Binkley, J. A. Pople and W. J. Hehre, *J. Am. Chem. Soc.*, 1980, **102**, 939.

48 A. E. Reed, R. B. Weinstock and F. Weinhold, *J. Chem. Phys.*, 1985, **83**, 735.

4514 | *Phys. Chem. Chem. Phys.*, 2022, **24**, 4504–4514

This journal is © the Owner Societies 2022